Measurement of the ^{24}Mg$(p,t)^{22}$Mg reaction and implications for the ^{21}Na$(p,\gamma)^{22}$Mg stellar reaction rate

N. Bateman,[1,3,4] K. Abe,[2] G. Ball,[3] L. Buchmann,[3] J. Chow,[4] J. M. D'Auria,[1] Y. Fuchi,[5] C. Iliadis,[6] H. Ishiyama,[5] K. P. Jackson,[3] S. Karataglidis,[7] S. Kato,[8] S. Kubono,[2] K. Kumagai,[2] M. Kurokawa,[9] X. Liu,[2] S. Michimasa,[2] P. Strasser,[9] and M. H. Tanaka[5]

[1]*Simon Fraser University, Burnaby, Canada V5A 1S6*

[2]*Center for Nuclear Study, University of Tokyo (CNS), RIKEN Campus, Hirosawa 2-1, Wako, Saitama 31-0198, Japan*

[3]*TRIUMF, Vancouver, Canada V6T 2A3*

[4]*University of Toronto, Toronto, Canada M5S 1A7*

[5]*IPNS, KEK, Tsukuba 305-0801, Japan*

[6]*The University of North Carolina, Chapel Hill, North Carolina 27599-3255*

[7]*Theory Division, Los Alamos National Laboratory, Los Alamos, New Mexico 87545*

[8]*Yamagata University, Yamagata 990-0021, Japan*

[9]*RIKEN, Hirosawa 2-1, Wako, Saitama 31-0198, Japan*

(Received 18 August 2000; published 21 February 2001)

Levels in ^{22}Mg between 4 and 7 MeV excitation energy have been populated in a high-resolution study of the ^{24}Mg$(p,t)^{22}$Mg reaction. Two new states have been observed at energies $E_x = 5090$ and 6323 keV, while two states were observed at 5962 and 6046 keV. The precision in measured excitation energies for several other ^{22}Mg levels has been improved substantially. In addition, a new state at 8141 keV was observed in ^{23}Mg. Using spin and parity restrictions from the present and previous work, we discuss $T=1$ analog state assignments of $A=22$ nuclei below 7 MeV excitation energy. The implications for the rate of the stellar reaction ^{21}Na$(p,\gamma)^{22}$Mg which takes part in hydrogen burning during nova outbursts are presented.

DOI: 10.1103/PhysRevC.63.035803 PACS number(s): 21.10.Pc, 25.40.Hs, 26.30.+k, 27.30.+t

I. INTRODUCTION

Classical nova outbursts are believed to be the result of thermonuclear runaways on the surfaces of white dwarfs accreting hydrogen-rich matter in close binary systems. Observations of the elements Ne, Na, Al, Mg, S, and Ar in certain nova ejecta have led to the important discovery of a new nova class, the so-called ONeMg novae. The observed heavy element enrichments can be explained by assuming an underlying ONeMg(C) white dwarf, i.e., a white dwarf resulting from cores of massive stars that have experienced core carbon burning. In this scenario initially abundant O, Ne, and Mg isotopes are mixed into the hydrogen burning envelope and are converted by explosive hydrogen burning nucleosynthesis to heavier nuclei with masses $A=20-40$. For a recent review, see Ref. [1]. Although current models explain gross properties of observed nova outbursts, a number of fundamental problems associated with the ONeMg white dwarf mass, the masses of accreted and ejected matter, and the mixing mechanism between white dwarf matter and accreted material, remain to be solved.

It has been suggested [2] that ONeMg novae produce observable amounts of the radioactive isotope ^{22}Na. In the ejected nova shells, the radioisotope ^{22}Na β decays with a half-life of 2.6 years to ^{22}Ne, leading to the emission of 1.275 MeV γ rays. Hydrodynamical computations estimate that the average yield of ^{22}Na per ONeMg outburst amounts to $10^{-9}-10^{-7}$M$_\odot$ [2–4], sufficiently high that nearby novae should produce γ-ray intensities that are detectable at Earth. At present, neither balloon-borne instruments nor detectors on-board satellites were able to detect ^{22}Na γ rays from novae (see, for example, Ref. [5]). However, several nearby novae will be targets for the future International Gamma-Ray Astrophysical Laboratory (INTEGRAL) mission with significantly improved detection sensitivity compared to previous measurements. It has to be emphasized that the detection of ^{22}Na γ rays from novae would impose important constraints on theoretical models of nova outbursts and their role in galactic nucleosynthesis.

A reliable prediction of ^{22}Na synthesis in nova outbursts requires knowledge of several key thermonuclear reaction rates. It has been shown recently [4] that one of the most important reactions in this respect is the proton capture on ^{21}Na. Depending on the magnitude of the ^{21}Na$+p$ reaction rate as compared to the β-decay rate of ^{21}Na, the radioisotope ^{22}Na is produced either by the reaction sequence ^{21}Na$(p,\gamma)^{22}$Mg$(\beta^+\nu)^{22}$Na or by ^{21}Na$(\beta^+\nu)^{21}$Ne$(p,\gamma)^{22}$Na. In fact, a relatively small ^{21}Na $+p$ rate favors the latter path and thus delays the production of ^{22}Na until the envelope is expanding and cooling down. As a result, an increased number of ^{22}Na nuclei survives the nova outburst [4].

The target nucleus ^{21}Na is unstable ($T_{1/2}=22.5$ s) and a direct measurement of its proton capture rate has not yet been attempted. However, such an experiment using inverse kinematics and requiring the use of an accelerated radioactive ^{21}Na beam is in preparation at the ISAC facility at TRIUMF. Until direct cross section measurements of the ^{21}Na$+p$ reaction are performed, indirect experimental techniques, supported by theoretical considerations, have to be applied in order to estimate the reaction rates. Such estimates are presented in Jose *et al.* [4] and Wiescher *et al.* [6]. These

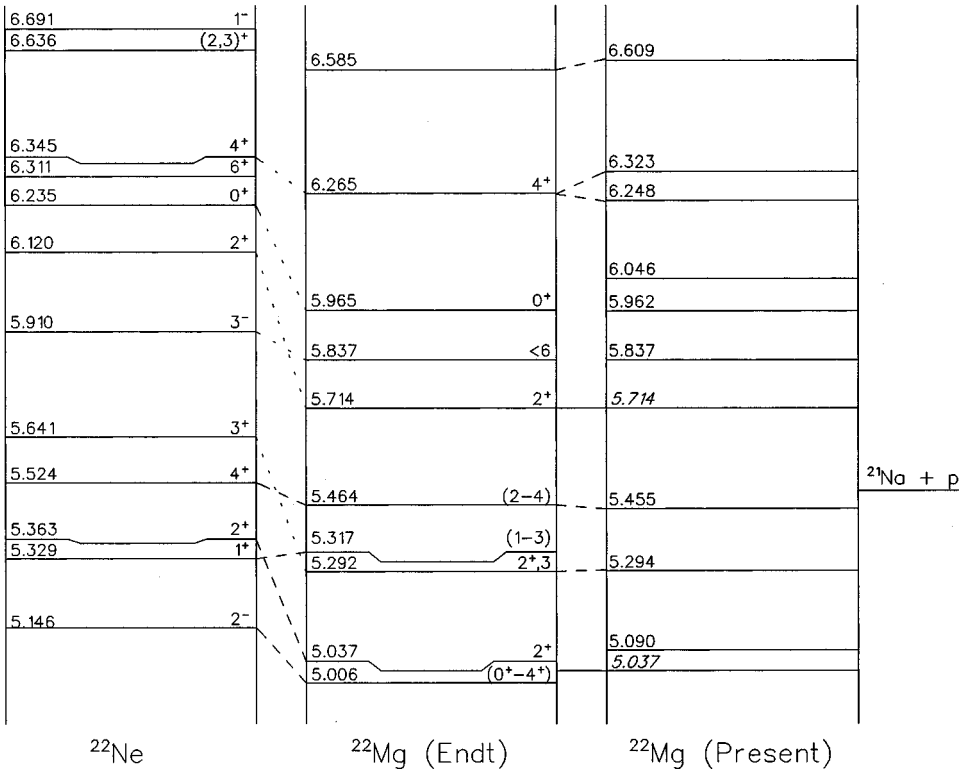

FIG. 1. Level diagrams of $T=1$ nuclei for $A=22$. Left, ^{22}Ne, from Ref. [7]; center, ^{22}Mg, from Ref. [7]; right, ^{22}Mg levels observed in the present work. Levels at 5.006 and 5.317 MeV states are not expected to be populated by a (p,t) reaction as they probably have unnatural parity. The mirror assignments between ^{22}Ne and ^{22}Mg noted with long-dashed lines are from Ref. [18]. Those noted with dotted lines are from Ref. [7], but are not present in the more recent compilation [18]. However these assignments have been used in all ^{21}Na$(p,\gamma)^{22}$Mg rate calculations.

authors took contributions of three resonances and the direct capture process into account. Resonance energies were calculated using ^{22}Mg excitation energies measured in two-nucleon transfer reactions (see Ref. [7]). Little experimental information is available regarding proton and γ-ray partial widths of these resonances and, therefore, reaction rate estimates were based on systematic nuclear trends and correspondences of ^{22}Mg states with analog levels in ^{22}Ne and ^{22}Na.

It is important to note that analog state assignments of isospin triplet states in $A=22$ nuclei are uncertain since for several known ^{22}Ne levels the corresponding mirror states in ^{22}Mg are missing, implying large uncertainties for the deduced ^{21}Na$+p$ capture reaction rates. Figure 1 displays levels of ^{22}Mg in the region of interest for the ^{21}Na$(p,\gamma)^{22}$Mg reaction. In the present work, we have reinvestigated the ^{24}Mg$(p,t)^{22}$Mg reaction with special emphasis on the detection of missing ^{22}Mg levels. Studies with radioactive beams and extended gas targets become more feasible when the required beam energy for a resonance reaction is known with higher precision than the energy loss in the target. Therefore, the energies of levels important for the proton capture rate have been remeasured to reduce their uncertainty. We have also performed shell model calculations in order to clarify the nuclear structure properties of states that enter into the calculation of the reaction rates.

The experimental equipment used in the present measurements is described in Sec. II. In Sec. III we discuss the data analysis. Our experimental ^{22}Mg excitation energies are presented in Sec. IV. Spin and parity assignments of ^{22}Mg levels are discussed in Sec. V. In Sec. VI we present correspondences of $T=1$ analog states in the $A=22$ system. The shell-model calculations are discussed in Sec. VII. New estimates of reaction rates are presented in Sec. VIII and conclusions are given in Sec. IX. Throughout this work, all quantities are given in the laboratory system unless mentioned otherwise.

II. EXPERIMENTAL EQUIPMENT AND PROCEDURES

The experiment was performed on the QDD spectrometer at Center for Nuclear Study at the University of Tokyo [8] which allowed measurement of the triton spectrum with high resolution. The focal plane detector described in Ref. [9] was used in which position sensitive wires were added behind the ΔE regions (see Fig. 2). The detector consists of a gas chamber and a plastic scintillator behind the chamber. In the gas

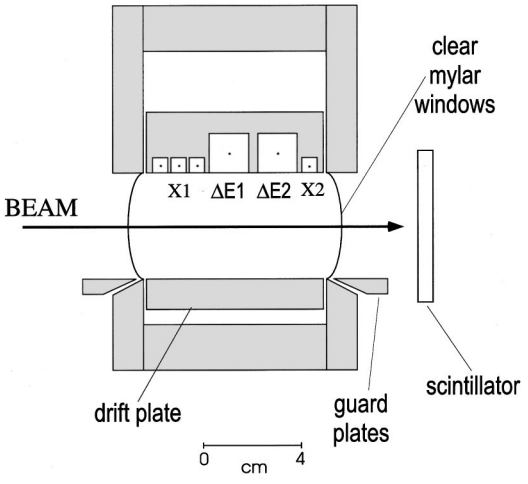

FIG. 2. Side-cross-sectional view of the focal plane detector. The entrance and exit windows of the gas counter are 3.5 cm in height and are covered with 12.5-μm Mylar foils.

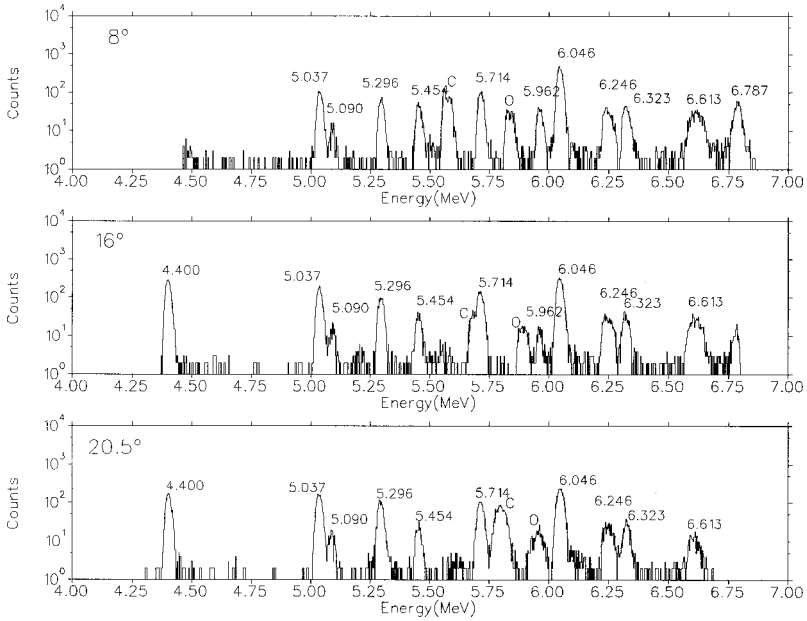

FIG. 3. Triton spectra from the three angles. Peaks marked with energies (in MeV) are the result of the $^{24}Mg(p,t)^{22}Mg$ reaction; peaks marked C and O are known contaminant lines from $^{12}C(p,t)^{10}C$ and $^{16}O(p,t)^{14}O$. Several smaller peaks were also produced by $^{16}O(p,t)^{14}O$.

chamber, charge is collected from four regions. In the front and at the back are position sensitive regions and the charge is read off both ends of the wires in these regions. Between the two regions are two ΔE regions from which charge is also collected. Although the detector can be moved to adjust the focus for kinematic shifts, we kept the position of the detector and the spectrometer magnetic fields constant throughout the experiment.

The proton beam from the CNS-SF cyclotron was maintained at a nominal laboratory energy of 37.925 MeV, and the beam tune was not adjusted during the run. Typical beam currents were 100 nA. The target was a $\geqslant$99.9% isotopically enriched ^{24}Mg metal foil of a nominal thickness of 290 $\mu g\,cm^{-2}$. Carbon and enriched ^{26}Mg foil targets were used to check for contaminants. Tritons were measured at lab angles of 8°, 16°, and 20.5°. The entrance aperture of the spectrometer was 5 mSr. However, to prevent protons from scattering from the target frame into the spectrometer, we used a second aperture to define the scattering angle in the scattering chamber. This limited our solid angle to 2 mSr.

To confirm that the beam was centered in the chamber, before and after the 20.5° run, we measured scattering from a Mylar target. This angle was chosen so that protons scattered elastically from ^{1}H nuclei would have the same rigidity as those scattered inelastically from the first excited state of ^{12}C. A comparison of the centroids of these two peaks shows that the difference between the effective scattering angle and the spectrometer angle was less than 0.3°.

The ^{24}Mg target thickness was verified during the run. In the data taken at each angle it was possible to resolve the peak from the $^{16}O(p,\alpha)^{13}N_{g.s.}$ reaction into two peaks, one corresponding to the reaction taking place in the oxygen layer on the front of the target, and one to the reaction taking place in the layer on the back. For the 8° data set it was also possible to do the same for the peaks due to $^{12}C(p,t)^{10}C(3.35MeV)$. The measured energy loss in the target was consistent with TRIM calculations of energy loss in a target of the nominal thickness to within 20%.

The stability of the experiment within each run was checked by monitoring the position of the strong peak from the $^{24}Mg(p,d)^{23}Mg$ reaction at 5.984 MeV in excitation. This position was stable to considerably better than 1 channel, or 2 keV in ^{22}Mg excitation energy.

III. DATA ANALYSIS

A. Position and energy calibration

In all of the runs we observed protons, deuterons, tritons and α particles in the detector. The energy lost in the front wire region gave the cleanest measure of ΔE. Hence this signal was used, along with the position in the front wire region, the energy lost in the scintillator, and the time between the scintillator and the rf signal as our primary particle identification. Two-dimensional gates allowed us to separate each particle group cleanly. One-dimensional gates on the other signals (back wire position, drift time, other ΔE signals) were used to further clean up the spectra. The final triton spectra are shown in Fig. 3. Our measured energy resolution is about 25 keV in terms of ^{22}Mg excitation, which is consistent with the expected energy loss in the target.

Position calibration of the focal plane was difficult for several reasons. The spectrometer bite extended from 4.3 to 6.9 MeV in ^{22}Mg excitation energy. There are not enough ^{22}Mg states of well-known energy in this region to provide an effective internal calibration. While the stability of the calibration of the spectrometer and detector within each run was very good, we were not able to confirm the stability of the calibration between runs, so we decided to calibrate all of the runs independently.

The deuteron group from the $^{24}Mg(p,d)^{23}Mg$ reaction provided a large number of calibration lines (see Fig. 4). We observed over thirty isolated lines between 5.2 and 8.5 MeV in excitation from this reaction at each angle, spread across the focal plane. Almost all of these states have excitation energies that are known to better than 6 keV. Because of the

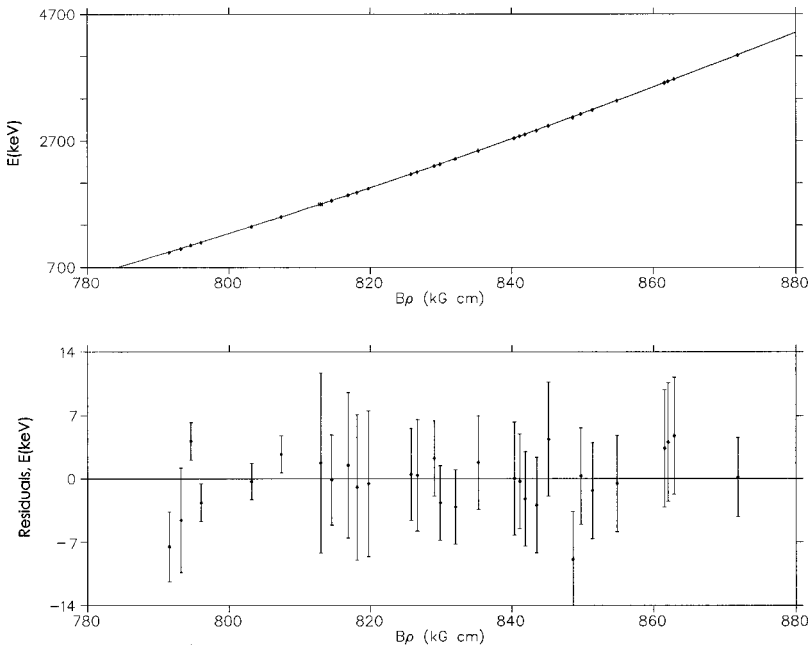

FIG. 4. Deuteron calibration of ^{23}Mg states for the 20.5° data set; fit (above), and residuals (below). $B\rho$ is calculated from kinematics and from energy losses in the target. The error bars in the residual plot reflect the uncertainty in the peak centroid and in the excitation energy of the various states, i.e., they represent the horizontal and vertical error bars added in quadrature.

different masses of the outgoing particles this corresponds to an uncertainty of less than 4 keV in the ^{22}Mg excitation energy scale.

However, although the centroids of the deuteron lines were determined very accurately, they are not ideal calibration lines. The size of the position signals for deuterons and tritons is quite different because of their different energy losses in the front wire region. We could not see any dependence of the position on the signal size, but even an unobservable effect could have a significant effect on the ^{22}Mg energies deduced from any deuteron calibration. To avoid this problem, we have used a somewhat unconventional procedure to adapt the deuteron calibration to the triton spectra.

At each angle the position along the focal plan was calibrated with known deuteron peaks from the ^{24}Mg(p,d) ^{23}Mg reaction. The corresponding rigidities were fit with a quadratic expression using TRIM calculations to determine energy loss in the target. The quadratic term derived from the detailed fit of the deuterons was used in determining the energies of tritons. Two states in ^{22}Mg at 5.7139 ± 0.0012 and 5.0370 ± 0.0014 MeV [7] were used as calibration lines.

Excitation energies at the three angles are listed in Table I. The uncertainties are discussed below. The agreement between the energies determined at the different angles is excellent. This demonstrates that all of the observed peaks are due to states in ^{22}Mg. If they were due to contaminants we would deduce different excitation energies at each angle. The only correlations between the different data sets come from the use of the same excitation energies for the two triton calibration lines (and to a much lesser extent the use of the same deuteron calibration lines).

B. Statistical errors

To determine the best energy for each observed state in ^{22}Mg from our data set we needed to address possible correlations between the uncertainties shown in Table I. In the following analysis the uncertainties on the fitted peak channels (ch_i, ch_a, ch_b) are considered to be ''statistical'' errors which is to say that they are uncorrelated, and other errors are considered to be systematic. For the data at each angle we determined the covariance matrix from the statistical uncertainties. The matrix elements are given by

$$M_{ii}^{\theta} = \left(\frac{\partial E_x^{i\theta}}{\partial \mathrm{ch}_i}\right)^2 \sigma_i^2 + \left(\frac{\partial E_x^{i\theta}}{\partial \mathrm{ch}_a}\right)^2 \sigma_a^2 + \left(\frac{\partial E_x^{i\theta}}{\partial \mathrm{ch}_b}\right)^2 \sigma_b^2 \qquad (1)$$

for the diagonal terms, and by

$$M_{ij}^{\theta} = \frac{\partial E_x^{i\theta}}{\partial \mathrm{ch}_a}\frac{\partial E_x^{j\theta}}{\partial \mathrm{ch}_a}\sigma_a^2 + \frac{\partial E_x^{i\theta}}{\partial \mathrm{ch}_b}\frac{\partial E_x^{j\theta}}{\partial \mathrm{ch}_b}\sigma_b^2 \qquad (2)$$

for the off-diagonal terms. θ labels the data sets from each angle, σ_i is the uncertainty in ch_i, σ_a is the uncertainty in ch_a, and σ_b is the uncertainty in ch_b where a and b are the two triton lines used for calibration.

TABLE I. ^{22}Mg excitation energies (keV) found from separate calibrations at each angle. The uncertainties include both statistical and systematic effects.

8°	16°	20.5°
	4399.0(5.3)	4400.5(5.2)
5089.5(1.9)	5090.9(1.8)	5089.1(1.6)
5296.5(1.3)	5296.5(1.3)	5295.0(1.2)
5454.8(1.3)	5454.3(1.4)	5454.5(1.3)
5961.1(2.4)	5964.4(2.8)	
6044.6(2.9)	6048.6(3.2)	6046.3(3.0)
6244.3(4.9)	6251.0(5.3)	6246.2(5.0)
6321.6(5.8)	6325.7(6.2)	6322.7(5.9)
6613.5(10.2)	6621.9(10.9)	6604.7(10.3)
6787(14)		

TABLE II. Covariance matrix for the energies of the seven fitted states; units are keV^2. The values have been scaled up to account for χ^2/ν (1.905). Systematic uncertainties are not included, and in general are the dominant uncertainties.The values of the diagonal elements of the correlation matrix imply that the energies at the different angles are generally consistent at the level of 1 keV or better.

	5.09	5.30	5.45	5.96	6.05	6.25	6.32
5.09	0.796	0.0290	0.0217	−0.00610	−0.0108	−0.0227	−0.0272
5.30	0.0290	0.124	0.0411	0.0469	0.0491	0.0511	0.0522
5.45	0.0217	0.0411	0.314	0.0939	0.100	0.115	0.122
5.96	−0.00610	0.0469	0.0939	0.842	0.276	0.339	0.364
6.05	−0.0108	0.0491	0.100	0.276	0.351	0.377	0.406
6.25	−0.0227	0.0511	0.115	0.339	0.377	1.11	0.503
6.32	−0.0272	0.0522	0.122	0.364	0.406	0.503	0.979

We then simultaneously fit the data with one excitation energy for each state. We do this by minimizing

$$\chi^2=\sum_{\theta}\sum_{i,j}(E_x^{i\theta}-E_x^{if})(M_{ij}^{\theta})^{-1}(E_x^{j\theta}-E_x^{jf}), \qquad (3)$$

where E_x^{if} is the fitted energy of state i.

The two ^{22}Mg states near the ends of the detector (the 4.40 and 6.59 MeV states) were excluded from the fit, because of possible nonlinear distortion effects at the detector windows. With the remaining seven lines we get $\chi^2/\nu=1.905$ for 13 degrees of freedom. The statistical uncertainties from this fit were scaled up to account for the high χ^2. The covariance matrix for these seven states is shown in Table II.

C. Systematic errors

To test the effect of systematic uncertainties we have repeated the fitting procedure while varying individual parameters. Changing the value of the beam energy by 75 keV in our fit left all of the energies within 0.2 keV of their original values. As a result the uncertainty in the beam energy was neglected. Similarly, changing the value of all of the scattering angles by 0.5° also left all of the energies within 0.2 keV of their original values, and the uncertainty in the angle has been neglected. We also performed a calculation with the target thickness set to zero, which left all the excitation energies within 0.1 keV of their initial values. Finally the Q values of the ^{24}Mg$(p,t)^{22}$Mg and ^{24}Mg$(p,d)^{23}$Mg energies were varied by one standard deviation. The change in excitation energy was smaller than 0.01 keV, so this uncertainty was also neglected.

Other systematic uncertainties that have been considered are the error resulting from the extrapolation from deuterons to tritons, the uncertainty introduced by using only the energies of the 5.037 and 5.714 MeV states, the uncertainty introduced by the assumption of a quadratic calibration of the focal plane detector, and the effect of finite angular distribution of the scattered tritons on the focal plane calibration. Our uncertainties are listed in Table III. For completeness we also estimate the dependence of the excitation energy of each state on the excitation energies of the calibration states and this is shown in Table IV. This dependence is an outcome of our analysis and not a part of it.

IV. EXPERIMENTAL EXCITATION ENERGIES

Our measured ^{22}Mg excitation energies are listed in column 1 of Table V. Previous experimental results below $E_x=7$ MeV are shown in columns 2–7. Compiled excitation energies [7] based on these previously obtained values are displayed in the last column. Corresponding states have been arranged in Table V in the same rows according to energy compatibility arguments. For most levels our results agree with previously reported excitation energies. Note that the present energy uncertainties are far smaller compared to the results of previous two-nucleon transfer studies, and that our errors are comparable in magnitude to the γ-ray spectroscopy work of Ref. [12]. Two new levels [7] were observed at $E_x=5090$ and 6323 keV while two levels were seen for the first time near 6 MeV ($E_x=5962$ and 6046 keV, see discussion below). The state at 5090 keV might correspond to the weakly populated level at $E_x=5130\pm35$keV reported in the (^{3}He,n) work of Ref. [10]. The levels at 5317 and 5837 keV have not been observed in the present work and hence these

TABLE III. Uncertainties in the energies (keV) of the seven fitted states. $\sigma_{\rm stat}$ is the uncertainty due to the uncertainty in peak centroids (from Table II). $\sigma_{A_2}^{\rm corr}$ is the uncertainty due to the use of the quadratic terms in the fit from the deuterons, assuming these terms are fully correlated. σ_{E_x} is the uncertainty due to the error in the energies of the calibration lines. $\sigma_{\rm cub}$ is the uncertainty introduced when a cubic term is added to the fit, $\sigma_{d\sigma/d\Omega}$ is the uncertainty from the angular distributions, and $\sigma_{\rm tot}$ is the total error for each state determined by adding all in quadrature. The uncertainty in scattering angle, beam energy, and target thickness can be neglected.

E_x	$\sigma_{\rm stat}$	$\sigma_{A_2}^{\rm corr}$	σ_{E_x}	$\sigma_{\rm cub}$	$\sigma_{d\sigma/d\Omega}$	$\sigma_{\rm tot}$
5089.7	0.90	0.19	1.39	0.15	0.21	1.7
5295.7	0.36	0.63	1.33	0.45	0.27	1.6
5454.3	0.57	0.64	1.28	0.43	0.32	1.6
5961.9	0.92	1.42	1.76	0.17	0.11	2.5
6045.8	0.59	2.09	1.99	0.12	0.24	3.0
6246.4	1.05	4.13	2.57	1.09	0.25	5.1
6322.6	0.99	5.07	2.80	1.07	0.29	6.0

TABLE IV. Dependence of the seven fitted states on the excitation energies of the calibration lines.

$E_x \pm \sigma_{tot}$ (keV)	$\partial E_x / \partial E_x^{5.71}$	$\partial E_x / \partial E_x^{5.04}$
5089.7±1.7	0.075	0.929
5295.7±1.6	0.367	0.621
5454.3±1.6	0.600	0.396
5961.9±2.5	1.396	−0.396
6045.8±3.0	1.533	−0.536
6246.4±5.1	1.883	−0.879
6322.6±6.0	2.013	−1.011

might be states of unnatural parity. The weighted-average excitation energies including previous and present work are shown in column 8 of Table V.

A few previously measured ^{22}Mg level energies are shown in parentheses in Table V and have not been used for the weighted averages in column 8. In these cases, single levels with large excitation energy errors have been reported previously that are shown in the present work to be doublets. It should be emphasized that we disregard in Table V the level at 5006 keV that has only been observed by Ref. [12]. We find no compelling evidence for the existence of this state, since it was proposed [12] based upon indirect evidence of Ref. [13], it was only present as a weak peak in one $n\gamma$-coincidence spectrum and was not observed in any of the $\gamma\gamma$-coincidence spectra (see Fig. 2 and Table I of Ref. [12]).

The two triton peaks displayed in Fig. 3, corresponding to the levels at 6249 and 6609 keV (Table V), respectively, exhibit larger widths compared to other peaks. The former peak corresponds probably to a doublet, whereas the latter peak is either caused by a level with a broad natural width or by a multiplet of states (see discussion in Sec. V).

In addition to the new states that we have seen in ^{22}Mg, we have also observed a new state in ^{23}Mg. In both the 8° and 16° spectra we observed three states between 8.1 and 8.2 MeV. Our deuteron calibration gives energies of 8.142, 8.168, and 8.195 MeV for the 8° data, and 8.141, 8.170, and 8.197 MeV for the 16° data. From Ref. [18] the known states are at 8.166±.002 and 8.193±0.008 MeV. We therefore deduce there is a state in ^{23}Mg at an excitation energy of 8.141±0.005 MeV (error similar to that observed for the other two states).

V. SPIN AND PARITY ASSIGNMENTS OF ^{22}Mg STATES

In this section we discuss spin and parity assignments (or restrictions) for levels in ^{22}Mg below $E_x = 7$ MeV. As a first step we reevaluated available experimental information from the literature. The results are listed in columns 2–5 of Table VI. One has to be especially careful with certain assignments that have been reported in previous two-nucleon transfer work. The reason is that for some levels values of the transferred orbital angular momentum have been assigned that are already based in part on analog level and shell-model assignments. The results are then (wrongly) interpreted by compilers as experimental information and are used subsequently

TABLE V. Experimental excitation energies (keV) in ^{22}Mg.

(p,t) present	$(^3\mathrm{He},n)$ Ref. [10]	(p,t) Ref. [11]	$(^3\mathrm{He},n\gamma)$ Ref. [12]	$(^3\mathrm{He},n\gamma)$ Ref. [14]	$(^3\mathrm{He},n)$ Ref. [15]	$(^{16}\mathrm{O},\ ^6\mathrm{He})$ Ref. [17]	adopted [g] present	adopted previous [a]
4399.8±4.2	4378±35	4417±27	4401.9±1.5	4399±2		4408±12	4400.9±1.2	4400.9±1.4
			5006±2 [c]					5006±2
5037.0 [b]	5032±30	5057±31	5037.0±1.4		5030±30	5029±12	5037.0±1.4	5037.0±1.4
5089.7±1.7	5130±35						5089.7±1.7	
5295.7±1.6	5286±30	5313±32	5290±2	5296±3	5330±50	5272±9	5293.5±1.1	5292±3
			5317±5				5317±5	5317±5
5454.3±1.6	5433±25		5464±5				5455.2±1.5	5464±5
5713.9 [b]	5699±20	5738±35	5714.4±1.5	5713±2	5680±30	5711±13	5713.9±1.2	5713.9±1.2
			5837±5				5837±5	5837±5
5961.9±2.5	5945±20 [f]				5980±30 [f]		5961.9±2.5	
6045.8±3.0		6061±37				6041±11	6045.6±2.9	5965±25
6246.4±5.1	6263±20 [d]	(6281±33) [d]	(6298±50) [d]		(6220±50) [d]	6255±10	6248.2±4.5 [e]	6267±15
6322.6±6.0		(6281±33) [d]	(6298±50) [d]		(6220±50) [d]		6322.6±6.0	
6613±7	6573±20	6645±44				6606±11	6608.5±5.6	6585±35
6787±14	6770±20	6836±44			6760±90	6767±20	6780.4±9.6	6783±19

[a]Reference [7].

[b]Used for calibration in the present work.

[c]Disregarded in present work; evidence for existence of this level in Ref. [12] is not convincing since it is based on a single observed γ-ray peak in $n\gamma$-coincidence spectrum.

[d]Doublet at $E_x = 6249$ and 6323 keV not resolved; quoted values have not been used for weighted average in column 8.

[e]Probably a doublet (see text).

[f]Assignment ambiguous (see text); quoted values have not been used for weighted average in column 8.

[g]Weighted average of columns 1–7.

TABLE VI. Spin and parity assignments of ^{22}Mg states.

E_x [a]	(^{3}He,$n\gamma$) Ref. [12]	(^{3}He,$n\gamma$) Ref. [14]	(^{3}He,n) Refs. [10,15]	(p,t) Ref. [11]	(p,t) present [l]	adopted assignment
0			0^+	0^+		0^+
1246	2^+ [b]		[i]	[i]		2^+
3308	(2,4) [c]	$\pi=+$ [h]	[i]	4^+		4^+
4402	2^+ [d]	$\pi=+$ [h]		[i]	$\pi=N$	2^+
5006 [e]						
5037	$(1,2^+)$ [f]		2^+	[i]	$\pi=N$	2^+
5090						
5294	(2^+-4^+) [f]	$(2^+,3)$ [h]	[h]		$\pi=N$	$(2^+, 3^-)$
5317	$(1,2^+)$ [f]					$(1,2^+)$
5455	(2^+-4^+) [f]				$\pi=N$	$(2^+, 3^-, 4^+)$
5714	$(1,2^+)$ [f]		2^+	[i]	$\pi=N$	2^+
5837	(2^+-4^+) [f]					(2^+-4^+)
5962			(0^+) [j]		$\pi=N$	$\pi=N$
6046				(0^+)	$\pi=N$	0^+
6248	[g]		(4^+)		$\pi=N$ [k]	[k]
6323	[g]				$\pi=N$	$\pi=N$
6609					$\pi=N$	$\pi=N$
6781					$\pi=N$	$\pi=N$

[a]From column 8 of Table V.
[b]From measured γ-ray angular correlation and τ_m.
[c]From measured γ-decay, γ-ray angular correlation, and τ_m.
[d]From measured γ-decay and γ-ray angular correlation.
[e]Disregarded; see Sec. IV.
[f]From γ decay and application of ''Dipole or $E2$ rule'' (see text).
[g]One of these states corresponds to 6298 keV level observed in Ref. [12].
[h]From measured γ-ray transition strength and τ_m.
[i]DWBA description of data not convincing.
[j]See text for assignment; assumes same state populated in (^{3}He,n) studies.
[k]Probably a doublet (see text).
[l]N denotes level of natural parity.

for spin and parity restrictions. Such ''cyclic reasoning'' has been carefully avoided in the present work.

Only in one particular case listed in Table VI have we made reference to the shell-model and analog structure. It has been shown in the present work that two levels exist in ^{22}Mg at 5962 and 6046 keV. Only the latter state has been populated in the previous (p,t) study by [11] and the measured excitation energy of $E_x=6061\pm37$ keV agrees with our result. On the other hand, the (^{3}He,n) studies of Refs. [10,15] report levels at $E_x=5945\pm20$ keV and 5980 ± 30 keV, respectively, and an assignment of these levels based on energy arguments alone is not definitive (Table V). The measured angular distributions in both (^{3}He,n) studies support the assignment $J^\pi=0^+$ for their observed level. The measured angular distribution in the (p,t) experiment [11] also implies $J^\pi=0^+$. Neither shell-model calculations nor the structure of the ^{22}Ne analog nucleus predicts the existence of two 0^+ levels in this region of excitation energy, but this is also not definitive. Chen [17] observes a state at 6041 ± 11 keV, and no state at 5960 keV, in studies of a ^{12}C(^{16}O, ^{6}He)^{22}Mg reaction. This reaction should only populate natural parity states also. The only conclusion consistent with all data (particularly the stated experimental errors) is that two different states are observed in the present (p,t) studies and the state at 6046 keV is not the same state observed in the (^{3}He,n) studies. [If the state at 5962 is the same state populated in the (^{3}He,n) studies, then it is 0^+.]

For the levels at 5037, 5294, 5317, 5455, 5714, and 5837 keV populated in γ-ray spectroscopy work we also obtain spin-parity assignments that are different from previously reported results. In these cases we used measured γ-ray branching ratios [12] and applied the ''dipole or $E2$-rule'' [7]. Note that this rule is valid only for high-lying levels (i.e., any level above, say, the 20th). Strictly speaking, this argument does not apply to the present cases. However, it has to be kept in mind that the γ-ray branches reported by Ref. [12] are rather strong and, consequently, the decay of these levels will most likely proceed via $E1$, $M1$, or $E2$ transitions.

Although no angular distributions have been measured here, the present results also provide spin-parity restrictions for ^{22}Mg states. We have assumed natural parity for all levels that are strongly populated in the present two-nucleon transfer measurement (column 6 of Table VI).

TABLE VII. Isospin triplet states ($T=1$) in $A=22$ nuclei. (Experimental information for ^{22}Ne and ^{22}Na from Refs. [7,18].)

^{22}Ne		^{22}Na		^{22}Mg		shell–model [d]	
E_x (keV)	J^π	E_x^* [a] (keV)	J^π	E_x [c] (keV)	J^π [b]	E_x (keV)	J_n^π
0	0^+	0	0^+	0	0^+	0	0_1^+
1275	2^+	1295	2^+	1246	2^+	1368	2_1^+
3358	4^+	3414	4^+	3308	4^+	3378	4_1^+
4456	2^+	4517	2^+	4402	2^+	4455	2_2^+
5146	2^-	5302	2^-	5090		5053	2_1^-
5329	1^+	5338	$(0-3^+)$	5317	$(1,2^+)$	5437	1_1^+
5363	2^+	5433	$(1,2)^+$	5037	2^+	5032	2_3^+
5524	4^+	5532	$(0-4)^+$	5455	$(2^+, 3^-, 4^+)$	5480	4_2^+
5641	3^+	5585		5837	(2^+-4^+)	5635	3_1^+
5910	3^-	5672	$(0-3)^-$	5294	$(2^+, 3^-)$	5636	3_1^-
6120	2^+	5894	$(1,2)^+$	5714	2^+	6179	2_4^+
6235	0^+	6177	$(0,1)^+$	6046	0^+	6344	0_2^+
6311	6^+					6397	6_1^+
6345	4^+	6341	(3^+-5^+)			6431	4_3^+
6636	$(2,3)^+$	6582	(2^+-4^+)			6520	3_2^+
6691	1^-					6880	1_1^-
6819	2^+	6814	2^+			6574	2_5^+
6854	1^+	6751	1^+			6663	1_2^+

[a]With $E_x^*=E_x-657$ keV.
[b]From Table VI.
[c]From Table V.
[d]See Sec. VII.

The adopted quantum numbers (or restrictions) are listed in column 7 of Table VI. The quoted results are based on experimental information. Note that the β-delayed proton decay work of Ref. [16] is not very useful for purposes of spin-parity assignments since protons have not been measured in coincidence with decay γ rays (in ^{21}Na). Therefore, it is difficult to decide if the observed proton decays populate the ^{21}Na ground state or excited states.

The broad level at 6249 keV observed in the present work (Sec. IV and Fig. 3) has a measured width of 26 ± 6 keV and is most likely a doublet. Suppose for a moment that we have observed a triton group populating a single ^{22}Mg level corresponding to a resonance energy of $E_R^{\text{c.m.}}\approx745$ keV and a width of $\Gamma\approx\Gamma_p=26\pm6$ keV. The single-particle width (assuming $C^2S=1$) for such a resonance amounts to $\Gamma_{sp}=16$, 4, and 0.2 keV for orbital angular momenta of $l=0,1$, and 2, respectively. Only the assumption of a *s*-wave resonance, implying $J^\pi=1^+$ or 2^+, can be consistent with the experimentally observed width. However, the shell-model spectroscopic factors for 1^+ or 2^+ states are much smaller than unity (Sec. VII). Thus we conclude that we probably have observed an unresolved doublet in ^{22}Mg at $E_x\approx6.25$ MeV.

VI. ANALOG STATE ASSIGNMENTS

In this section we discuss the correspondence of $T=1$ analog states in the mass $A=22$ system. Our analog assignments are presented in Table VII and are based on experimental information (E_x and J^π) of ^{22}Mg levels presented in the previous sections and in Tables V and VI. An interpretation of the ^{22}Mg level structure in terms of the shell model is presented in the next section. As mentioned in the previous section, we disregard the 5006 keV state reported by Ref. [12].

The ^{22}Mg levels at $E_x=0$, 1246, 3308, 4402, 5037, 5714, and 6046 keV (Tables V and VI) have unambiguous J^π values and thus their analog state correspondence is straightforward.

The level at 5317 keV $(1,2^+)$ most likely has a spin and parity of 1^+. There is no other available 2^+ state in this region of excitation energy and the ^{22}Ne level structure indicates that the first 1^- level is expected to occur above 6.5 MeV.

The newly found level at 5090 keV is only weakly populated in the present work, implying possibly an unnatural parity assignment. Together with energy compatibility arguments the assignment 2^- seems most likely.

For the state at 5294 keV $(2^+, 3^-)$ there is no 2^+ level available in this excitation energy range and, therefore, corresponds probably to the first 3^- isospin triplet. According to the spin and parity assignments of Table VI, the 5837 keV (2^+-4^+) level most likely corresponds to the first 3^+ isospin triplet since all other listed states are of natural parity. This state is not observed in the present (p,t) study, supporting the assumption of unnatural parity.

For the 5455 keV $(2^+, 3^-, 4^+)$ state neither 2^+ nor 3^-

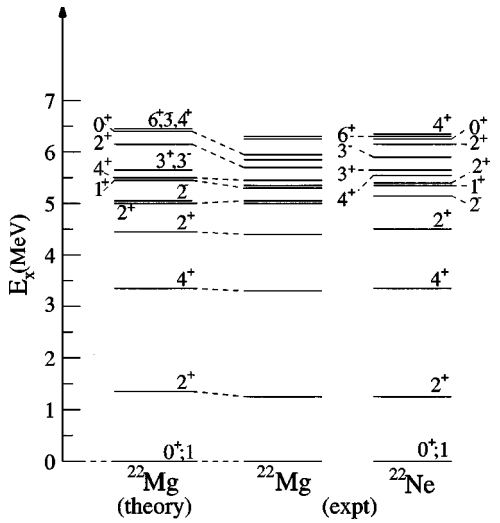

FIG. 5. Calculated and experimental energy levels for ^{22}Mg and ^{22}Ne. The experimental levels are taken from Ref. [21] and the present study.

levels are available in this region of excitation energy and, consequently, the most likely assignment is 4^+.

The remaining levels at 5962, 6249, 6323, 6609, and 6781 keV, listed in Tables V and VI, are difficult to assign. First, the $E_x = 6249$ keV state might be a doublet as discussed in the previous section. Second, for these levels the available J^π restrictions are rather poor (Table VI) and thus assignments based purely on excitation energy arguments are uncertain.

VII. SHELL-MODEL CALCULATIONS FOR $A=22$

Shell-model calculations for the mass-22 system were performed with the code OXBASH in a complete $(0+1)\hbar\omega$ space using the (isospin-conserving) WBT interaction of Warburton and Brown [20]. This procedure allows for a consistent calculation of both positive parity $(0\hbar\omega)$ and negative parity $(1\hbar\omega)$ states with the same interaction and within the same configuration space. All states below 10 MeV with $J \leqslant 8$ were included in the calculation.

The calculated levels of ^{22}Mg below 7.0 MeV are listed in column 7 of Table VII and are displayed in Fig. 5, together with experimental ^{22}Mg and ^{22}Ne levels. The calculated ^{22}Mg spectrum agrees with that obtained from experiment. The 2_1^- (5053 keV) and the 2_3^+ (5032 keV) shell-model states are inverted in the calculation compared to the corresponding experimental levels in ^{22}Ne. In these two cases, the agreement between experimentally assigned and calculated ^{22}Mg level energies is excellent (columns 5 and 7 of Table VII). The 3_1^+ and 3_1^- shell-model states both lie at $\approx$5.63 MeV due to an incidental degeneracy in the calculation. The 6_1^+ and 4_3^+ states are predicted to be at 6397 and 6431 keV, respectively, in approximate agreement with the corresponding experimental level energies in ^{22}Ne.

Shell-model spectroscopic factors are compared in Table VIII with the corresponding experimental values obtained in the ^{21}Ne$(d,p)^{22}$Ne neutron-transfer study of Ref. [19]. It can be seen that the agreement is excellent for levels with reported experimental C^2S values. Furthermore, our shell-model calculation predicts very small spectroscopic factors for all states with no reported experimental C^2S values. The only exception is the shell-model state at 6431 keV (4_3^+, $C^2S_{\rm SM} = 0.12$). Note however, that no acceptable angular distribution fit could be found in Ref. [19] for the corresponding ^{22}Ne level at 6345 keV (Table VII), presumably because of the close proximity of the 6311 keV level and the relatively poor experimental energy resolution of about 25 keV.

TABLE VIII. Comparison of measured spectroscopic factors and mean lifetimes with shell-model results for states in ^{22}Mg (for correspondence of experimental ^{22}Mg and ^{22}Ne levels with shell-model states, see Table VII).

$E_x^{\rm SM}$ [a] (keV)	J_n^π [a]	$C^2S(l,l+2)$ [b] theory	$C^2S(l,l+2)$ [b] experiment [c]	τ_m theory	τ_m experiment [d]
0	0_1^+	0.13	$\leqslant$0.20		
1368	2_1^+	0.009,0.98	0.65	2.5 ps	3.0 ± 1.2 ps [e]
3378	4_1^+	0.03	0.05	0.31 ps	0.29 ± 0.07 ps
4455	2_2^+	0.06,0.19	0.054,0.14	3.9 fs	$<$30 fs
5032	2_3^+	0.24,0.07	0.31,	9.0 fs	$<$100 ps
5053	2_1^-	0.004,0.014		1.0 ps	
5437	1_1^+	0.05,0.59	0.05,0.46	2.8 fs	$<$25 ns
5480	4_2^+	0.32	0.25	18.1 fs	$<$100 ps
5635	3_1^+	0.16	0.07	5.8 fs	$<$25 ns
5636	3_1^-	0.001,0.004		0.54 ps	63 ± 20 fs
6179	2_4^+	0.01,0.001		2.9 fs	40 ± 15 fs
6344	0_2^+	0.05		9.8 fs	
6397	6_1^+			20.0 fs	
6431	4_3^+	0.12		2.6 fs	
6520	3_2^+	0.12	0.10	2.3 fs	

[a] From columns 7 and 8 of Table VII.
[b] Single-nucleon transfer spectroscopic factors; l and $l+2$ denote different possible orbital angular momenta.
[c] From ^{21}Ne$(d,p)^{22}$Ne study of Ref. [19].
[d] Measured lifetimes of ^{22}Mg levels adopted from Ref. [7].
[e] The value $\tau_m = 30\pm12$ ps quoted in Ref. [7] is likely a misprint.

For the calculation of mean lifetimes and γ-ray branching ratios, as we are using a $(0+1)\hbar\omega$ model, an estimate of the degree of core polarization is required. We have calculated the effective charge needed from the $B(E2)$ value of the first 2^+ state in ^{22}Mg, located at 1246 keV [7]. Its measured lifetime is reported as 2.1 ps [21], implying a $B(E2)$ value of $129.3\,e^2\,{\rm fm}^4$. The latter value is reproduced within our model for a polarization charge of $1.1\,e$. This result is subsequently used in all calculations of lifetimes and γ-ray branching ratios of ^{22}Mg states below 6.5 MeV.

Experimental and shell-model lifetimes of ^{22}Mg levels are compared in columns 5 and 6 of Table VIII. Unfortunately, values of τ_m have been measured in a few cases only and experimental upper limits are reported for most ^{22}Mg levels. For the low-lying levels, the calculated lifetimes agree with the data. However, discrepancies exist for the shell-model states at 5636 keV (3_1^-) and 6179 keV (2_4^+),

TABLE IX. Experimental and calculated γ-ray branching ratios (in %) for ^{22}Mg states. (For correspondences of experimental ^{22}Mg levels with shell-model states, see Table VII. The experimental B_γ values are adopted from Ref. [12] and are given in parentheses.)

	J_f^π	0_1^+	2_1^+	4_1^+	2_2^+	2_3^+
J_i^π	$E_x^{\rm SM}$ (keV)	0	1368	3378	4455	5032
2_1^+	1368	100 (100)				
4_1^+	3378		100 (100)			
2_2^+	4455		100			
		(8±4)	(87±4)	(5±4)		
2_3^+	5032	24	76			
		(12±4)	(88±4)			
2_1^-	5053	2	94		4	
1_1^+	5437	68	31		1	
		(30±15)	(70±15)			
4_2^+	5480		3	97		
			(70±10)	(30±10)		
3_1^-	5636	3	3		85	9
				(60±10)	(40±10)	
3_1^+	5635		81	19		
			(80±15)	(20±15)		
2_4^+	6179	4	85		11	
		(13±3)	(87±3)			

corresponding to ^{22}Mg levels at 5294 and 5714 keV, respectively (Table VII). For the 3_1^- level, the calculated lifetime amounts to 0.54 ps, about an order of magnitude longer than the measured value of 63±20 fs [7]. The calculated γ-ray decay of this level proceeds predominantly via a $E1$ transition to the 2_2^+ state (see Table IX) and the discrepancy may be due to limitations in the model space in exhausting the $E1$ sum rule. For the 2_4^+ level, the calculated lifetime amounts to 2.9 fs which is shorter than the measured value of 40±15 fs. However, the latter result was extracted from an experimental $F(\tau)$ value close to unity with a rather large uncertainty [$F(\tau)=0.87\pm0.04$ [14]]. According to Table I of Ref. [14], the measured value of $F(\tau)=0.90\pm0.03$ for the 2_2^+ level resulted already in an upper limit of $\tau_m<30$ fs. Therefore, part of the discrepancy might be explained by experimental difficulties in extracting relatively short lifetimes.

Calculated and measured γ-ray branching ratios are compared in Table IX. The latter values have been adopted from Ref. [12]. The agreement is excellent for the shell-model states at 1368 (2_1^+), 3378 (4_1^+), 4455 (2_2^+), and 5032 (2_3^+) keV. Measured and calculated B_γ values also agree well for the shell-model states at 5635 (3_1^+) and 6179 (2_4^+) keV and, therefore, support our assignments to the experimentally observed ^{22}Mg levels at $E_x=5837$ and 5714 keV, respectively (Table VII).

VIII. ASTROPHYSICAL IMPLICATIONS

The stellar reaction rates $N_A\langle\sigma v\rangle$ of ^{21}Na$(p,\gamma)^{22}$Mg can have contributions from resonances and the direct capture into final ^{22}Mg states. The reaction rate (in units of reactions $s^{-1}mole^{-1}cm^3$) for isolated narrow resonances is given as a function of temperature T_9 (in units of GK) by the expression [22]

$$N_A\langle\sigma v\rangle = 1.54\times10^{11}(\mu T_9)^{-3/2}\sum_i \omega\gamma_i \exp\left(-11.605\frac{E_i}{T_9}\right), \tag{4}$$

where the reduced mass μ is in amu and the strengths $\omega\gamma_i$ and center-of-mass energies E_i of the resonances are in MeV. The stellar rates for the ^{21}Na$(p,\gamma)^{22}$Mg reaction have been calculated using the analog assignments of ^{22}Mg states presented in Sec. VI (see also Table VII). For stellar temperatures of $T\leqslant0.4$ GK it is sufficient to consider resonances located within about 0.5 MeV of the proton threshold in ^{22}Mg ($Q_{p\gamma}=5501$ keV [23]). Resonance energies $E_R^{\rm c.m.}=212$, 336, 460, and 541 keV are calculated from the experimental excitation energies $E_x=5714$, 5837, 5962, and 6046 keV listed in Table V. Resonance strengths $\omega\gamma$ are determined by proton and γ-ray partial widths Γ_p and Γ_γ. Proton partial widths were calculated using the procedure described in Ref. [24]. Single-particle spectroscopic factors for the $E_R^{\rm c.m.}=212$, 336, and 541 keV resonances have been adopted from shell-model calculations (Sec. VII and Table VIII). The analog assignment of the $E_x=5962$ keV state is uncertain and an upper limit of Γ_p has been estimated assuming a p-wave resonance and $C^2S\leqslant1$. An s-wave resonance would imply $J^\pi=2^+$ (the assignment $\pi=N$ in Table VI rules out the value 1^+), but all 2^+ states in this excitation energy region have already been assigned to experimental ^{22}Mg levels (Table VII).

Gamma-ray partial widths for the $E_R^{\rm c.m.}=212$, 336, and 541 keV resonances have been calculated by using the measured lifetimes of ^{22}Ne mirror states (Table VII and Ref. [18]), corrected for the difference in γ-ray transition energies. For the $E_R^{\rm c.m.}=460$ keV resonance we adopted the value $\Gamma_\gamma\approx1$ eV as an order-of-magnitude estimate. A summary of estimated resonance properties for ^{22}Mg states near the proton threshold is presented in Table X. Note that for the $E_R^{\rm c.m.}=212$ keV resonance ($E_x=5714$ keV in ^{22}Mg, corresponding to 2_4^+) the experimental mean lifetime (Table VIII) amounts to $\tau_m=40\pm15$ fs [7]. The measured value implies a total width of $\Gamma=1.6^{+1.0}_{-0.4}\times10^{-2}$ eV, consistent with our estimated total width of $\Gamma=\Gamma_p+\Gamma_\gamma=2.6\times10^{-2}$ eV (Table X). The resulting stellar reaction rate contribution of narrow resonances is listed in column 2 of Table XI.

The (nonresonant) direct capture (DC) contribution into all ^{22}Mg bound states was determined following the formalism described in Ref. [25]. The radial wave functions for the bound final states were calculated by using a Woods-Saxon potential ($r=1.25$ fm and $a=0.65$ fm). The well depth is chosen to reproduce the binding energy of each final state. For the calculation of the initial state radial wave function we have employed hard-sphere phase shifts. The total DC cross section is given by an incoherent sum over orbital angular momenta l_i and l_f for all incoming and outgoing partial waves involved,

TABLE X. Parameters of low-energy resonances in ^{21}Na$(p,\gamma)^{22}$Mg.

E_x [a] (keV)	$E_R^{\text{c.m.}}$ [b] (keV)	J_n^π [c]	C^2S [d]	l	Γ_p [e] (eV)	Γ_γ [f] (eV)	$\omega\gamma$ [g] (eV)
5713.9±1.2	212.4	2_4^+	0.01,0.001	0,2	4.6×10^{-3} [h]	2.2×10^{-2} [h]	2.4×10^{-3}
5837±5	335.5	(3_1^+)	0.16	2	4.7×10^{-2}	$\geqslant 6.6\times10^{-2}$	3.2×10^{-2} [i]
5961.9±2.5	460.4		$\leqslant 1$ [j]	(1)	$\leqslant 1.6\times10^{2}$	≈ 1 [j]	$\leqslant 3.7\times10^{-1}$ [j]
6045.6±2.9	541.4	0_2^+	0.05	2	8.8×10^{-1}	1.6×10^{-3}	2.0×10^{-4}

[a]From Table V.
[b]Calculated from column 1 using $Q_{p\gamma}=5501.5\pm1.5$ keV [23].
[c]Assignments adopted from Table VII.
[d]Shell-model spectroscopic factors (Table VIII).
[e]Proton partial widths calculated from C^2S values in column 4 using Eq. (7) in Ref. [24].
[f]Gamma-ray partial widths, calculated from measured lifetimes of mirror states in ^{22}Ne (see Table VII and Ref. [18]), and corrected for differences in γ-ray transition energies.
[g]With $\omega\gamma=(2J_R+1)\Gamma_p\Gamma_\gamma/8\Gamma$.
[h]In agreement with the measured mean lifetime of this state $\tau_m=40\pm15$ fs (Table VIII), corresponding to a total width of $\Gamma=1.6^{+1.0}_{-0.4}\times10^{-2}$eV (see Sec. VIII).
[i]Value of resonance strength restricted by relation $\omega\Gamma_p\Gamma_\gamma/(\Gamma_p+\Gamma_\gamma)\leqslant\omega\gamma\leqslant\omega\Gamma_p$.
[j]Analog assignment uncertain; upper limit for $\omega\gamma$ has been estimated with assumptions $J^\pi=1^-$, $l=1$, $C^2S\leqslant1$, and $\Gamma_\gamma\approx1$eV (see Sec. VIII).

$$\sigma_{\text{total}}^{\text{DC}}=\sum_{l_i,l_f} C^2S(l_f)\sigma_{\text{theo}}^{\text{DC}}(l_i,l_f). \tag{5}$$

The spectroscopic factors for the bound ^{22}Mg states were adopted from shell-model calculations (Table VIII). The total DC cross section was converted into the astrophysical S factor

$$S(E)=\sigma(E)E\exp(2\pi\eta), \tag{6}$$

with η denoting the Sommerfeld parameter. For bombarding energies below 1 MeV the S factor can be expressed as

$$S(E)=7.9\times10^{-3}-3.4\times10^{-3}E+1.8\times10^{-3}E^2\ \text{MeV}\times\ b. \tag{7}$$

Our derived direct capture S factor is about 50% larger compared to the results of Ref. [6]. The stellar reaction rates for

TABLE XI. Stellar reaction rates for ^{21}Na$(p,\gamma)^{22}$Mg. (Reaction rates in units of reactions $s^{-1}mole^{-1}cm^3$; above $T=0.4$ GK the reaction rates become uncertain due to the unknown contribution of the $E_R^{\text{c.m.}}=460$ keV resonance.)

T (GK)	resonances [a]	DC [b]	recommended [c]	Ref. [6]	Ref. [4]
0.01		5.99×10^{-33}	5.99×10^{-33}	6.02×10^{-36}	6.02×10^{-36}
0.015	9.28×10^{-67}	8.52×10^{-28}	8.52×10^{-28}	9.55×10^{-31}	9.55×10^{-31}
0.02	4.19×10^{-49}	1.50×10^{-24}	1.50×10^{-24}	1.84×10^{-27}	1.84×10^{-27}
0.03	1.58×10^{-31}	1.74×10^{-20}	1.74×10^{-20}	2.47×10^{-23}	2.47×10^{-23}
0.04	8.56×10^{-23}	6.29×10^{-18}	6.29×10^{-18}	1.01×10^{-20}	1.01×10^{-20}
0.05	1.38×10^{-17}	4.12×10^{-16}	4.26×10^{-16}	5.14×10^{-18}	1.21×10^{-18}
0.06	3.88×10^{-14}	9.96×10^{-15}	4.88×10^{-14}	1.29×10^{-14}	1.62×10^{-15}
0.07	1.09×10^{-11}	1.26×10^{-13}	1.10×10^{-11}	3.80×10^{-12}	5.11×10^{-13}
0.08	7.28×10^{-10}	1.02×10^{-12}	7.29×10^{-10}	2.67×10^{-10}	3.76×10^{-11}
0.09	1.87×10^{-8}		1.87×10^{-8}	7.19×10^{-9}	1.05×10^{-9}
0.1	2.47×10^{-7}		2.47×10^{-7}	9.95×10^{-8}	1.46×10^{-8}
0.15	4.98×10^{-4}		4.98×10^{-4}	2.47×10^{-4}	3.56×10^{-5}
0.2	2.00×10^{-2}		2.00×10^{-2}	1.15×10^{-2}	1.59×10^{-3}
0.3	7.33×10^{-1}		7.33×10^{-1}	4.93×10^{-1}	7.75×10^{-2}
0.4	4.92×10^{0}		4.92×10^{0}	3.03×10^{0}	6.75×10^{-1}

[a]Contribution of narrow resonances.
[b]Contribution from direct capture.
[c]Total recommended rate from present work.

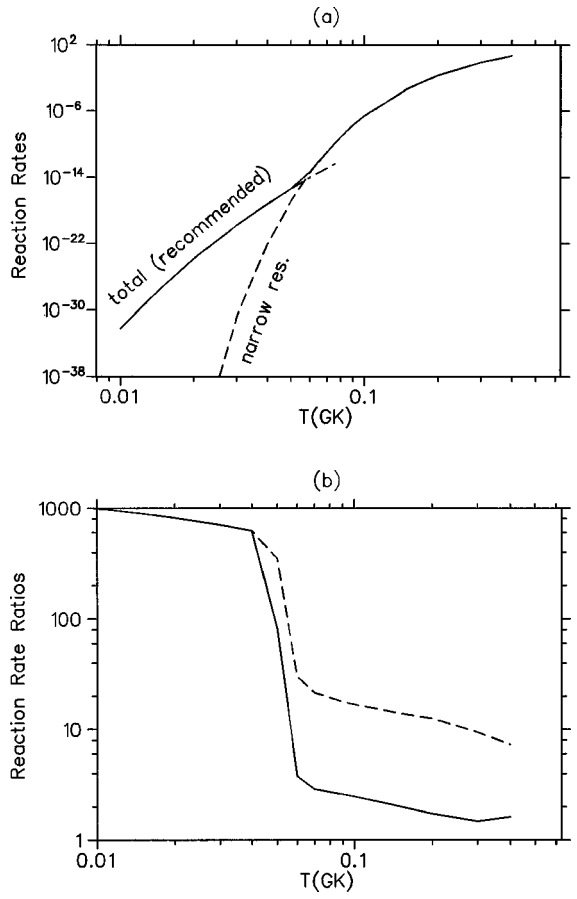

FIG. 6. (a) The total stellar rate ^{21}Na$(p,\gamma)^{22}$Mg reaction (bold) and the contribution from narrow resonances (dash). (b) Ratios of the reaction rates are shown as compared to previous studies (dashed line [4], solid line [6]).

the DC process, calculated by using the expressions for nonresonant reaction mechanisms [22], are listed in column 3 of Table XI.

The total stellar rates for ^{21}Na$+p$, which we recommend for use in stellar network calculations until results based on direct cross section measurements become available, are presented in column 4 of in Table XI and are displayed in Fig. 6 together with individual contributions. The direct capture process dominates the rates at low temperatures below $T=0.06$ GK. The $E_R^{\mathrm{c.m.}}=212$ keV resonance determines the reaction rates in the temperature region $T=0.06-0.4$ that is most important for nova nucleosynthesis. Above $T=0.4$ GK the rates become uncertain due to the unknown contribution of the $E_R^{\mathrm{c.m.}}=460$ keV resonance (Table X). The $E_R^{\mathrm{c.m.}}=336$ keV resonance increases the reaction rates at $T=0.4$ GK by only 25%. The $E_R^{\mathrm{c.m.}}=541$ keV resonance is negligible at all stellar temperatures.

The present reaction rates are compared in Fig. 6 to previous results of Refs. [6,4], which are also listed in columns 5 and 6 of Table XI. The previously derived values have been obtained by using systematic nuclear trends and different analog assignments for some of the states considered. For temperatures $T=0.1-0.4$ GK important in nova outbursts the present reaction rates deviate from the results of Refs. [6,4] by factors of ≈ 2 and ≈ 10, respectively. In the former work, an order-of-magnitude estimate $C^2S\approx 0.01$ was used for the calculation of Γ_p for all considered resonances. For the astrophysically most important $E_R^{\mathrm{c.m.}}=212$ keV resonance, their estimate[1] incidentally agrees with the present spectroscopic factor obtained from shell-model calculations (Table VIII). Consequently, the present and previous [6] reaction rates are in reasonable agreement. The results of the present work do not support the conclusion of an uncertain analog assignment for the ^{22}Mg state at 5714 keV, as has been claimed in Ref. [4]. These authors note that the measured spectroscopic factor of the ^{22}Na state at 6551 keV ($E_x^*=6551-657\,\mathrm{keV}=5894\,\mathrm{keV}$; Table VII) is too large ($C^2S\approx 0.1$ [27]) in order to agree with a presumably much smaller C^2S value of the analog state at 5714 keV in ^{22}Mg. They conclude that the analog assignments are uncertain and regard the $\omega\gamma$ value of Ref. [6] as an upper limit. Although one would expect similar spectroscopic factors for *mirror* states in ^{22}Ne and ^{22}Mg, one has to be very careful when comparing properties in isospin multiplets since isospin mixing in the $T_z=0$ nucleus (here ^{22}Na) can easily account for large variations of spectroscopic factors.

IX. CONCLUSIONS

A new study of the level energies in the nuclide, ^{22}Mg has been completed using a ^{24}Mg$(p,t)^{22}$Mg reaction. Several of these levels are important for radiative proton capture reactions on ^{21}Na occurring in a classic nova stellar explosion. These energies are now known to better precision which is important for planned future studies of the ^{21}Na$(p,\gamma)^{22}$Mg reaction using a radioactive beam at the TRIUMF-ISAC facility. Several new states were found and shell model calculations have been performed to help explain some of the properties and assignments of states. Improved rate estimates of this reaction were also performed.

ACKNOWLEDGMENTS

We thank B.A. Brown for his unpublished *sd*-shell model calculation of the positive parity states in ^{22}Mg and their properties, and for useful discussions. We also thank Alan Chen for providing data from his thesis. This work was supported in part by the Canadian funding agency NSERC, by the U.S. Department of Energy under Contracts No. DE-FG02-97ER41041 and W-7405-ENG-36, and by the Ministry of Education, Science, Sports, and Culture of Japan under Contract No. 10440070.

[1]Another paper by the authors of Ref. [26] reports for the $E_R^{\mathrm{c.m.}}=212$ keV resonance a $\omega\gamma$ value similar to our result. However, their estimates of proton width and angular momentum transfer are clearly in disagreement with our shell-model results (Table VIII). The source of the disagreement is the method applied in Ref. [26] of estimating reduced widths by using simple Thomas-Ehrmann shift calculations. The latter procedure yields very unreliable results, especially in the present case where the mirror states have small single-particle spectroscopic factors.

[1] R. D. Gehrz, J. W. Truran, R. E. Williams, and S. Starrfield, Publ. Astron. Soc. Pac. **110**, 3 (1998).
[2] A. Weiss and J. W. Truran, Astron. Astrophys. **238**, 178 (1990).
[3] S. Starrfield, J. W. Truran, M. Wiescher, and W. M. Sparks, Mon. Not. R. Astron. Soc. **296**, 502 (1998).
[4] J. Jose, A. Coc, and M. Hernanz, Astrophys. J. **520**, 347 (1999).
[5] A. F. Iyudin *et al.*, Astron. Astrophys. **300**, 422 (1995).
[6] M. Wiescher *et al.*, Astron. Astrophys. **160**, 56 (1986).
[7] P. M. Endt, Nucl. Phys. **A521**, 1 (1990).
[8] S. Kato, H. Hasegawa, and M. Tanaka, Nucl. Instrum. Methods **154**, 19 (1978).
[9] M. H. Tanaka, S. Kubono, and S. Kato, Nucl. Instrum. Methods **195**, 509 (1982).
[10] A. B. McDonald and E. G. Adelberger, Nucl. Phys. **A144**, 593 (1970).
[11] R. A. Paddock, Phys. Rev. C **5**, 485 (1971).
[12] C. Rolfs *et al.*, Nucl. Phys. **A191**, 209 (1972).
[13] M. H. Shapiro *et al.*, Nucl. Phys. **A144**, 17 (1970).
[14] H. Grawe, K. Holzer, K. Kändler, and A. A. Pilt, Nucl. Phys. **A237**, 18 (1975).
[15] W. P. Alford *et al.*, Nucl. Phys. **A457**, 317 (1986).
[16] B. Blank *et al.*, Nucl. Phys. **A615**, 52 (1997).
[17] A. Chen, Ph.D. thesis, Yale University, 2000.
[18] P. M. Endt, Nucl. Phys. **A633**, 1 (1998).
[19] P. Neogy, R. Middleton, and W. Scholz, Phys. Rev. C **6**, 885 (1972).
[20] E. K. Warburton and B. A. Brown, Phys. Rev. C **46**, 923 (1992).
[21] R. B. Firestone, *Table of Isotopes*, 8th ed. edited by Virginia S. Shirley (Wiley, New York, 1996).
[22] W. A. Fowler, G. R. Caughlan, and B. A. Zimmerman, Annu. Rev. Astron. Astrophys. **5**, 525 (1967).
[23] G. Audi and A. H. Wapstra, Nucl. Phys. **A595**, 409 (1995).
[24] C. Iliadis, Nucl. Phys. **A618**, 166 (1997).
[25] C. Rolfs, Nucl. Phys. **A217**, 29 (1973).
[26] M. Wiescher and K. Langanke, Z. Phys. A **325**, 309 (1986).
[27] J. D. Garrett, R. Middleton, and H. T. Fortune, Phys. Rev. C **4**, 165 (1971).